Silver-doped biphasic calcium phosphate/alginate microclusters with antibacterial property and controlled doxorubicin delivery

Article *in* Journal of Applied Polymer Science · December 2020

DOI: 10.1002/app.50433

CITATIONS
0

READS
29

12 authors, including:

Lei Nie
KU Leuven
51 PUBLICATIONS **493** CITATIONS
SEE PROFILE

Yi Sun
Universitair Ziekenhuis Leuven
76 PUBLICATIONS **801** CITATIONS
SEE PROFILE

Constantinus Politis
Universitair Ziekenhuis Leuven
463 PUBLICATIONS **2,910** CITATIONS
SEE PROFILE

Amin Shavandi
Université Libre de Bruxelles
90 PUBLICATIONS **875** CITATIONS
SEE PROFILE

Received: 22 September 2020 | Revised: 2 December 2020 | Accepted: 21 December 2020

DOI: 10.1002/app.50433

ARTICLE

Applied Polymer SCIENCE WILEY

Silver-doped biphasic calcium phosphate/alginate microclusters with antibacterial property and controlled doxorubicin delivery

Lei Nie[1,2] | **Yaling Deng**[3] | **Yingying Zhang**[1] | **Qiuju Zhou**[4] | **Qimin Shi**[5] | **Shengping Zhong**[5] | **Yi Sun**[2] | **Zhong Yang**[3] | **Meng Sun**[1,6] | **Constantinus Politis**[2] | **Amin Shavandi**[7]

[1]College of Life Sciences, Xinyang Normal University, Xinyang, China

[2]Department of Imaging & Pathology, University of Leuven and Oral and Maxillofacial Surgery, University Hospitals Leuven, Leuven, Belgium

[3]College of Intelligent Science and Control Engineering, Jinling Institute of Technology, Nanjing, China

[4]Analysis and Testing Center, Xinyang Normal University, Xinyang, China

[5]OMFS-IMPATH Research Group, Department of Biomedical Sciences, KU Leuven and Department of Oral and Maxillofacial Surgery, University Hospitals Leuven, Leuven, Belgium

[6]State Key Lab of Metal Matrix Composites, School of Materials Science and Engineering, Shanghai Jiao Tong University, Shanghai, China

[7]BioMatter unit - École polytechnique de Bruxelles, Université Libre de Bruxelles, Brussels, Belgium

Correspondence
Lei Nie, Department of Imaging and Pathology, University of Leuven and Oral and Maxillofacial Surgery, University Hospitals Leuven, Leuven 3001, Belgium
Email: nieleifu@yahoo.com; nielei@xynu.edu.cn

Yaling Deng, College of Intelligent Science and Control Engineering, Jinling Institute of Technology, Nanjing 211169, P.R. China.
Email: dengyaling1119@163.com

Amin Shavandi, BioMatter unit - École polytechnique de Bruxelles, Université Libre de Bruxelles, Avenue F.D. Roosevelt, 50 - CP 165/61, 1050 Brussels, Belgium.
Email: amin.shavandi@ulb.be

Funding information
National Natural Science Foundation of China, Grant/Award Number: 31700840; Six Talent Peaks Project in Jiangsu Province (CN), Grant/Award Number: 2019 05

Abstract

Biphasic calcium phosphate (BCP) based materials possessed with both excellent biocompatibility and antibacterial activity show potential advantages for biomedical applications. Here, the silver-doped BCP/Alginate ($_{Ag}$BA) microclusters were first fabricated using the double-emulsions method. First, BCP nanoparticles were incorporated into the alginate network to form BCP/Alginate microclusters via the emulsion process. Then, silver nanoparticles (AgNPs) were in situ involved in BCP/Alginate networks to obtain the final $_{Ag}$BA microclusters. Transmission electron microscopy and scanning electron microscopy confirmed that BCP nanoparticles and AgNPs were uniformly distributed in $_{Ag}$BA microclusters. The morphology of $_{Ag}$BA microclusters could be regulated by adjusting emulsion power, and microclusters using the medium powder (500 W) showed a regular spherical shape. Furthermore, CCK-8 analysis identified that $_{Ag}$BA microclusters were cytocompatible culturing with human bone marrow-derived mesenchymal stem cells. Qualitative antibacterial tests exhibited the excellent inhibition effects of $_{Ag}$BA microclusters against *Staphylococcus aureus* (Gram-positive) and *Escherichia coli.* (Gram-negative). Lastly, the doxorubicin (DOX)-loaded $_{Ag}$BA microclusters presented adjustable loading efficiency of DOX and controllable release profiles. The cumulative release could reach 73.3% after 72 h in PBS.

Lei Nie and Yaling Deng contributed equally to this work and considered as co-first authors.

The above results raised a new route for antibacterial microclusters development for biomedical applications.

KEYWORDS

biomedical applications, colloids, drug delivery systems, polysaccharides, nanoparticles, nanowires, and nanocrystals

1 | INTRODUCTION

Bone tissue engineering, as an effective therapeutic strategy, has addressed much attention in the development of dealing with therapies for bone regeneration/remodeling.[1] Bone scaffolds have been widely used as promising alternatives, such as polymers,[2,3] ceramics,[4] and their composites.[5] Bone scaffolds with cells and growth factors are aiming to repair or replacement of damaged and diseased parts of human bone. Meanwhile, effective drugs could be incorporated within scaffolds for treating or preventing infection (e.g., osteomyelitis), bone tumor, osteoporosis.[6] The antibacterial property is a critical characteristic desired to reduce implant failures by providing resistance against various bacterial infections to ensure long-term stability.[7,8] Such as antibiotics have been applied to treat bone disease caused by bacteria systematically.[9,10] Unfortunately, treatments are not always practical due to microbial resistance. The prolonged and extensive application of antibiotics over time has caused the emergence and increase of bacterial resistance.[11] The discovery of new antibiotics is still challenging due to the intrinsical resistance of the bacteria.[12] Therefore, new strategies to develop novel bactericidal agents have now become urgent to combat the emergence of multidrug-resistant.

Silver (Ag) has been used as bacterial disinfection for a long history in the form of metal and ions to treat injuries, wounds, and bacterial infections.[13] Mainly, silver nanoparticles (AgNPs) have been widely applied in biomedical applications, owing to the strong bactericidal effect against a wide range of bacteria with low cytotoxicity.[14–16] Additionally, AgNPs exhibit a substantial surface-area-to-volume ratio, achieving efficient antibacterial effects compared to those of other Ag-based salts and microscale silver particles.[17,18] However, the poor stability and dispersion of AgNPs limit their applications as antibacterial materials. Besides, AgNPs tend to aggregate to form larger-sized particles leading to the loss of antibacterial activities. One potential solution to overcome the aggregation is to fix or stabilize AgNPs on substrates, and such an approach also enhances its stability and antibacterial performance.[19] Some Ag-based hybrid nanostructures have been achieved and show superior antibacterial activities, such as AgNPs/ZnO,[20] AgNPs/ESM (eggshell membrane, ESM),[21,22] AgNPs/HA (hydroxyapatite, HA),[23] and AgNPs/SA (sodium alginate, SA),[24] and so on.

Alginate is a linear unbranded polysaccharide, forming by 1,4′-linked β-D-mannuronic acid and α-L guluronic acid residues.[25] Due to the inherent biodegradability, biocompatibility, and non-allergenic reactions of alginate,[26] it has been widely exploited in modern medicine, such as drug delivery application.[27,28] Several alginate-based composite microspheres, such as sodium alginate/carboxymethyl chitosan/collagen (SA/CMCS/Collagen) combined with berberine,[29] hydroxyapatite/sodium alginate/chitosan (HA/SA/CS) coated with Doxorubicin (DOX),[30] strontium-substituted hydroxyapatite/Alginate microspheres loaded with vancomycin,[31] displayed effective antibacterial activity, and the drug release could be regulated by pH, which was helpful to prevent infection in pre-hospital applications. In our previous studies, AgNPs-doped HA/Alginate nanocomposite microparticles and DT-GO (dithiol-modified) nanosheets reinforced alginate nanocomposite displayed an excellent cytocompatibility and antibacterial activity against Gram-negatively *Escherichia coli* (*E. coli*) and Gram-positive *S. aureus*.[23,32] Due to the roles of stabilizer and reductant for alginate, alginate could be effectively fabricated microparticles or microclusters for drug delivery and antibacterial.[33] There were a few reports on the fabrication of alginate composited with biphasic calcium phosphate (BCP) as a matrix for stabilizing AgNPs.

It was well-known that BCP possessed a unique balance between the stable HA and more soluble β-tricalcium phosphate (β-TCP),[34] which was known to be the osteoinductive material for bone tissue engineering due to the excellent biocompatibility, bioactivity, and effectiveness.[35,36] In recent years, the researchers have focused on the desired BCP-based materials, which could combine both therapy functions of drug-eluting and regeneration, bringing lots of benefits compared with conventional medical practice.[37] Due to the particular nanostructured surface topography and inner porosity, BCP-based materials were highly influential in the loading and prolonged-release drug molecules, such as BCP microspheres,[38] TOCNF (TEMPO-oxidized cellulose nanofiber) reinforced SA/β-TCP (sodium alginate/β-tricalcium phosphate) microspheres,[39] BCP/chitosan

composite scaffolds.[40] However, the fabrication of the BCP-based microclusters as bactericidal agents with good cytocompatibility was rarely reported.

In this work, we hypothesized that BCP nanoparticles could be composited with alginate polymer network to form microclusters via emulsion method, and then AgNPs were in situ incorporated in the formed BCP/alginate nanostructured hybrid microclusters, providing the antibacterial ability and cytocompatibility. A facile double-emulsion method using ultrasonic homogenizer was used to synthesize BCP-based microclusters. First, BCP nanoparticles were dispersed into the alginate network to form BCP/Alginate microclusters, according to previous reports.[23,41] Then AgNPs were in situ incorporated into BCP/Alginate microclusters to form $_{Ag}$BA microclusters. A schematic diagram of the preparation process for $_{Ag}$BA microclusters was shown in Figure 1. The antibacterial activities and the properties, as a potential doxorubicin carrier, were investigated systematically.

2 | EXPERIMENTAL SECTION

2.1 | Materials

Ammonia ($NH_3 \cdot H_2O$), and calcium nitrate tetrahydrate ($Ca[NO_3]_2 \cdot 4H_2O$) were purchased from Sino-Pharm Chemical Reagent Co., Ltd. Ascorbic acid and silver nitrate ($AgNO_3$) were purchased from Aldrich Co., Ltd. Ammonium phosphate dibasic ($[NH_4]_2HPO_4$) and sodium alginate (SA, AR, 90%, M/G = 1:2) were purchased from Macklin Biochemical Co., Ltd. DOX · HCl was obtained from URchem Co., Ltd. All the chemicals used in this manuscript were in analytical reagent level and used as received.

2.2 | Synthesis of BCP nanoparticles

The aqueous precipitation was used to prepare BCP nanoparticles according to our previous studies.[42,43] The mixed solution of $Ca(NO_3)_2 \cdot 4H_2O$ and $(NH_4)_2HPO_4$ solutions with a Ca/P mole ratio of 1.55 were prepared. The pH of the mixed solutions was adjusted to around 11 using the ammonia solution. After then, the mixed solutions were stirred for 4 h at room temperature (RT). The products were collected through centrifugation, cleaned with Millipore water several times, and dried at 80°C. Finally, the products were treated at 1125°C for 1 h using a muffle furnace. The BCP nanoparticles were treated using a ball grinding machine (FOCUCY, F-P2000), and then the stainless steel sieves (200 mesh sieve) was used to obtain the BCP nanoparticles with controlled size.

2.3 | Preparation of AgNPs-doped BCP/alginate ($_{Ag}$BA) microclusters

AgNPs-doped BCP/Alginate ($_{Ag}$BA) microclusters were fabricated using a double-emulsions method via ultrasonic homogenizer machine (SCIENTZ-IID, Ningbo

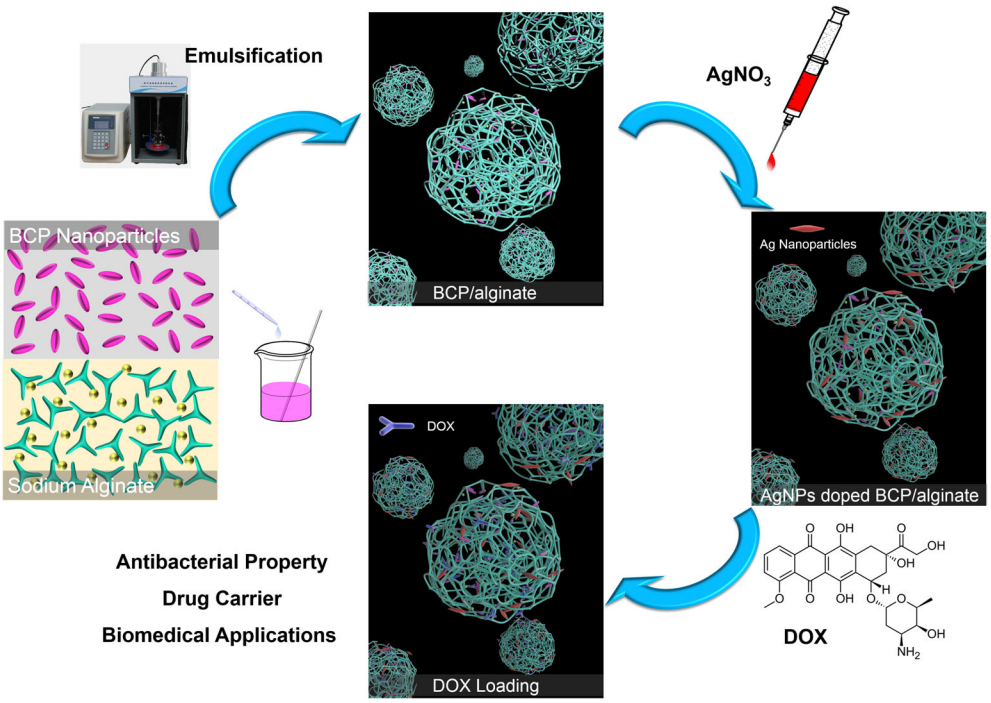

FIGURE 1 Schematic diagram of the preparation of silver nanoparticles-doped biphasic calcium phosphate/alginate ($_{Ag}$BA) microclusters with antibacterial property, as a doxorubicin carrier for biomedical applications [Color figure can be viewed at wileyonlinelibrary.com]

Xinzhi BioTech. Co., Ltd). In 0.84 mg of SA was dissolved in 80 ml of Millipore water to obtain solution A, and 0.51 mg of $AgNO_3$ was dissolved in 60 ml of Millipore water to acquire solution B. In 150 mg of BCP nanoparticles powder was added in 12 ml of solution A and emulsified using an ultrasonic homogenizer for 1 min, the power was set at 500 W. Then, 12 ml of solution B was injected into the emulsified solution A, and emulsified again for 1 min using the same power of 500 W. Afterward, 2 ml of 0.1 M ascorbic acid was added and kept for 10 min, and the final microclusters were centrifuged (3000 rpm) for 5 min and washed using Millipore water three times. Finally, after the freeze-dried, the microclusters designated were MPs-m was obtained. The designation of MPs-l, MPs-m, and MPs-h represented that the emulsified power of 300 W, 500 W, and 900 W, respectively, during both emulsion processes.

2.4 | Physicochemical characteristics

The morphology and composition of the prepared $_{Ag}$BA microclusters were observed by cold field emission-scanning electron microscopy (SEM, S4800) and FEI-transmission electron microscopy (TEM, Tecnai G2 F20) equipped with energy dispersive spectroscopy and elemental mapping accessories. Fourier transform infrared (FTIR) spectra of the samples were obtained by an FTIR spectrometer (PerkinElmer, Spectrum 2) that employed a potassium bromide pellet method. The FTIR spectra were collected in the region between 4000 and 500 cm^{-1}. The $_{Ag}$BA microclusters were analyzed using the X-ray diffraction (XRD, Rigaku Smartlab 9 kW diffractometer) with Cu Kα1 radiation over the range of 10–90°. The UV–Visible spectra were obtained using Ultraviolet–visible spectroscopy (UV–Vis, Lambda 950), the diffuse-reflectance spectrum (DRS) mode was used during the UV–Vis testing.

2.5 | Antimicrobial activity assay

Here, the antibacterial activity of $_{Ag}$BA microclusters was evaluated using two typical bacterial strains, including Gram-negative *E. coli* (ATCC 25922) and Gram-positive *Staphylococcus aureus* (*S. aureus*, ATCC 6538). Single overnight colonies of *E. coli* and *S. aureus* were revived from the glycerol stocks on the Luria-Bertani (LB) agar plate and transferred to tubes with sterilized liquid LB culture medium to construct a seed culture by growing at 37°C overnight with shaking (180 rpm). After then, the growing seed culture was diluted into flasks with fresh LB medium and cultured using the same condition. The growth of bacteria was monitored by checking the optical density at 600 nm (OD_{600}). Once OD_{600} reached 0.6, the broth was diluted to 2×10^6 CFU ml^{-1} with a sterile 0.9% NaCl solution. Then, cell suspension (50 μl) was evenly spread onto a 90 mm LB agar plate with sterile glass beads. A hole puncher was used to make the wells with a diameter of 4 mm, and 30 μl of $_{Ag}$BA microclusters with different concentrations were added as well. Finally, the growth of bacteria on the plates was incubated at 37°C for 12 h. On the other hand, OD_{600} of liquid culture of bacteria mixed with $_{Ag}$BA microclusters for 8 h was presented as complementary data to appraise its antibacterial activity. In 100 μl of microclusters, 10 ml of autoclaved LB medium, and 5 μl of seed cultures of *E. coli* and *S. aureus* were cultured into the tube at 37°C for 8 h, then OD_{600} of the cultured mixed solution was recorded using the visible spectrophotometer (VIS-7220 N, RAYLEIGH).

2.6 | Preparation of DOX-loaded $_{Ag}$BA microclusters

In 10 mg of DOX and 10 mg of $_{Ag}$BA microclusters were dispersed in 5 ml Millipore water and stirred for 24 h at RT. Then, the DOX loaded microclusters were separated by ultracentrifugation (20,000 g, ALLEGRA X-30R, B063222) for 1 h, washed three times using Millipore water to remove the unloaded DOX. Finally, the DOX-loaded $_{Ag}$BA microclusters were obtained after vacuum-dried treatment. Here, the encapsulation efficiency of DOX (E_{encaps}) was calculated by the following equation via UV–Vis spectrophotometer (Agilent Cary5000):

$$E_{encaps}\,(\%) = \left(M_{feed} - M_{residual}\right)/M_{feed} \times 100\%. \quad (1)$$

where M_{feed} was the total feed amount of DOX, and $M_{residual}$ was the amount in the solution after ultracentrifugation.

2.7 | Release profile of DOX

The release profiles of DOX-loaded $_{Ag}$BA microclusters, including MPs-l, MPs-m, and MPs-h, were investigated. In 1 mg of DOX-loaded $_{Ag}$BA microclusters was injected into a 20 kDa MWCO dialysis cassette (Thermo ScientificTM Slide-A-LyzerTM). Then, the cassette was placed in 80 ml of PBS containing 5% of BSA and stirred at 37°C; the pH of PBS was in the range of 7.35 ~ 7.45. Then, 100 μl of aliquots were collected and replaced with fresh PBS at predetermined hours. The cumulative release of DOX was measured and calculated via a UV–Vis spectrophotometer.

2.8 | Cell culture

Due to the potential applications in bone tissue engineering, the human bone marrow-derived mesenchymal stem cells (hBMSCs, Normal, Human, ATCC®PCS-500-012™) was used to evaluate the cytocompatibility of $_{Ag}$BA microclusters. Simultaneously, the lung cancer cell (A549 lung epithelial cells, ATCC®CCL-185™) was employed to investigate the cytotoxicity influence of DOX-loaded $_{Ag}$BA microclusters. According to ATCC instructions, hBMSCs were grown in Dulbecco's modified Eagle's medium (DMEM) (Sigma-Aldrich) supplemented with 10% fetal bovine serum (FBS), and 1% of a 100 mg/ml mixture of penicillin and streptomycin. A549 cells were grown in DMEM with 10% FBS, 100 U/ml penicillin, and 100 μg/ml streptomycin. Both hBMSCs and A549 cells were cultured in a humidified atmosphere of 5% CO_2 at 37°C and passaged using trypsinization. The culture medium was replaced every 2 days, all the cells at passage 5 for the next experiments.

2.9 | Cytocompatibility of $_{Ag}$BA microclusters and cytotoxicity of DOX-loaded $_{Ag}$BA microclusters

The cytocompatibility of $_{Ag}$BA microclusters (with hBMSCs) and cytotoxicity of DOX-loaded $_{Ag}$BA microclusters (against A549 cells) were quantitatively evaluated via Cell Counting Kit-8 (CCK-8) assay. In 1 ml of cell solution (1×10^5) was diluted into 24 ml and transferred into a 24-well plate (1 ml for each well), then a certain amount of microclusters dispersed in Millipore water was added. After culturing for 1 day, 3 days, and 5 days, the culture media was removed, 300 μl of fresh culture media and 30 μl of CCK-8 kit solutions were added and homogeneously mixed, then incubated at 37 °C for 4 h in a CO_2 incubator. Finally, the reaction solutions were transferred to a 96-well plate, and the optical density at 450 nm (OD_{450nm}) was recorded by a microplate reader (SpectraMax 190, Molecular Devices, USA).

2.10 | Statistical analysis

Each experiment was performed in triplicate if without a particular explanation, and all results were expressed as means ± SDs. The SPSS software package was used to perform statistical analyses, the homogeneity of variance was determined using Levene's test, and the comparison between different groups was performed using Tamhane Post Hoc tests. The statistical significance reported at a *p-value of <0.05 for 95% confidence, **$p < 0.01$ for 99% confidence, and ***$p < 0.001$ for 99.9% confidence.

3 | RESULTS

3.1 | Morphology of AgNPs-doped BCP/Alg ($_{Ag}$BA) microclusters

The double-emulsions approach was used to prepare AgNPs-doped BCP/Alginate ($_{Ag}$BA) microclusters. In this work, the ultrasound-based emulsification technique was employed, and the ultrasonic homogenizer with different emulsification power (300 W, 500 W, and 900 W) was performed. The morphology of $_{Ag}$BA microclusters was investigated by TEM first, as shown in Figure 2. The needle-shaped BCP crystallites (Figure 2(a)) were synthesized for the fabrication of $_{Ag}$BA microclusters in this work. The unregular clusters-shaped $_{Ag}$BA microclusters were obtained while the emulsification power was set at 300 W and 500 W, confirmed by TEM images of MPs-l and MPs-m exhibited in Figure 2(b-f). There are abundant round black nanoparticles, considered as AgNPs, that were observed and distributed on the surface of spherical-shaped microclusters at high magnification (Figure 2(e-f)). The average diameter of AgNPs is about 5.469 ± 0.798 nm, calculated via software ImageJ. Besides, the high-angle annular dark-field (HAADF) image of MPs-m was shown in Figure 2(g). The elemental mapping confirmed that the presence of oxygen (O), calcium (Ca) and phosphorus (P), and silver (Ag) uniformly distributed in the $_{Ag}$BA microclusters, proving that AgNPs and BCP nanoparticles were evenly incorporated into the alginate polymer network. However, while the emulsion power was increased to 900 W, the smaller size of $_{Ag}$BA microclusters (MPs-h) was observed in comparison with MPs-l and MPs-m, as shown in Figure 2(h-i).

On the other hand, SEM images of $_{Ag}$BA microclusters were used as complementary data to further investigate the morphology of $_{Ag}$BA microclusters as displayed in Figure 3. $_{Ag}$BA microclusters of MPs-l displayed the apparent agglomeration behavior and presented the irregular clusters-shape in Figure 3(a),(b), which was similar to TEM images in Figure 2(b),(c). In Figure 3(c),(d), a series of microclusters with a range of different sizes were observed. Those microclusters showed a regular spherical shape with surface roughness. MPs-h microclusters were irregular spherical shape with a rough surface with average diameter of 9.251 ± 1.708 μm as shown in Figure 3(e),(f). It has a smaller average diameter than MPs-m microcluster (about 15.979 ± 6.586 μm). SEM investigation confirmed that the emulsification

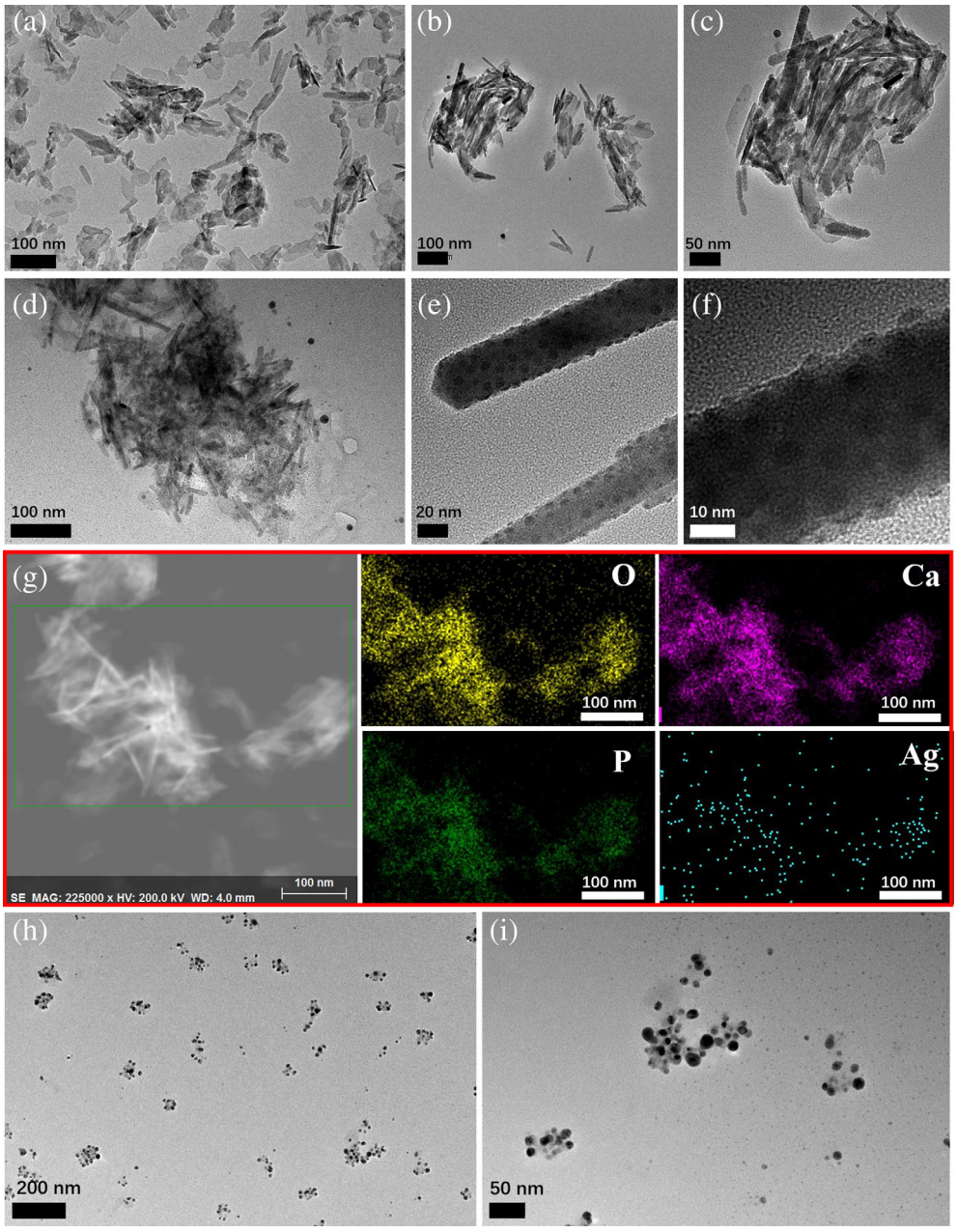

FIGURE 2 Morphology of BCP nanoparticles and $_{Ag}$BA microclusters prepared via ultrasonic homogenizer. TEM image of BCP nanoparticles (a) and TEM images at different magnifications of $_{Ag}$BA microclusters using different emulsification power, (b, c): MPs-l, 300 W; (d, e, f): MPs-m, 500 W; (h, i): MPs-h, 900 W. the high-angle annular dark-field (HAADF) image (g) for MPs-m was obtained, and the elemental mapping proved the presence of oxygen (O, yellow), calcium (ca, purple), phosphorus (P, green) and silver (Ag, blue) in $_{Ag}$BA microclusters. BCP, biphasic calcium phosphate; TEM, transmission electron microscopy [Color figure can be viewed at wileyonlinelibrary.com]

power had a significant influence on $_{Ag}$BA microclusters' morphology and size.

3.2 | Physicochemical characteristics of $_{Ag}$BA microclusters

Next, the physicochemical properties of $_{Ag}$BA microclusters were evaluated using Fourier Transform Infrared (FT-IR) spectroscopy, Ultraviolet–Visible (UV–Vis) absorption, and X-ray diffraction (XRD). The FTIR spectra of pure alginate and BCP nanoparticles were displayed in our previous works, thus they were not shown here.[32,35] The FTIR spectra of $_{Ag}$BA microclusters were shown in Figure 4(a). The characteristic absorption peaks observed at 3437, 1634, 1455, and 962 cm^{-1} correspond to -OH stretching vibration, C=O asymmetric stretching, C-O-C stretching vibration, C-O stretching vibration of alginate, respectively.[27,44] For studying the ion crosslinking process, the peaks at 1634 cm^{-1} and 1455 cm^{-1} of alginate (carboxylate group) are the most apparent characteristics.[45] The spectrum at 1032, 603, and 564 cm^{-1} are assigned to the specific peaks of phosphate group stretching and bending of BCP nanoparticles.[46] There was a slight shift for $_{Ag}$BA microclusters peaks from 1070 to 1032 cm^{-1}, compared with that of pure BCP nanoparticles. This shift was based on the carboxylate group in alginate and phosphate groups in BCP,

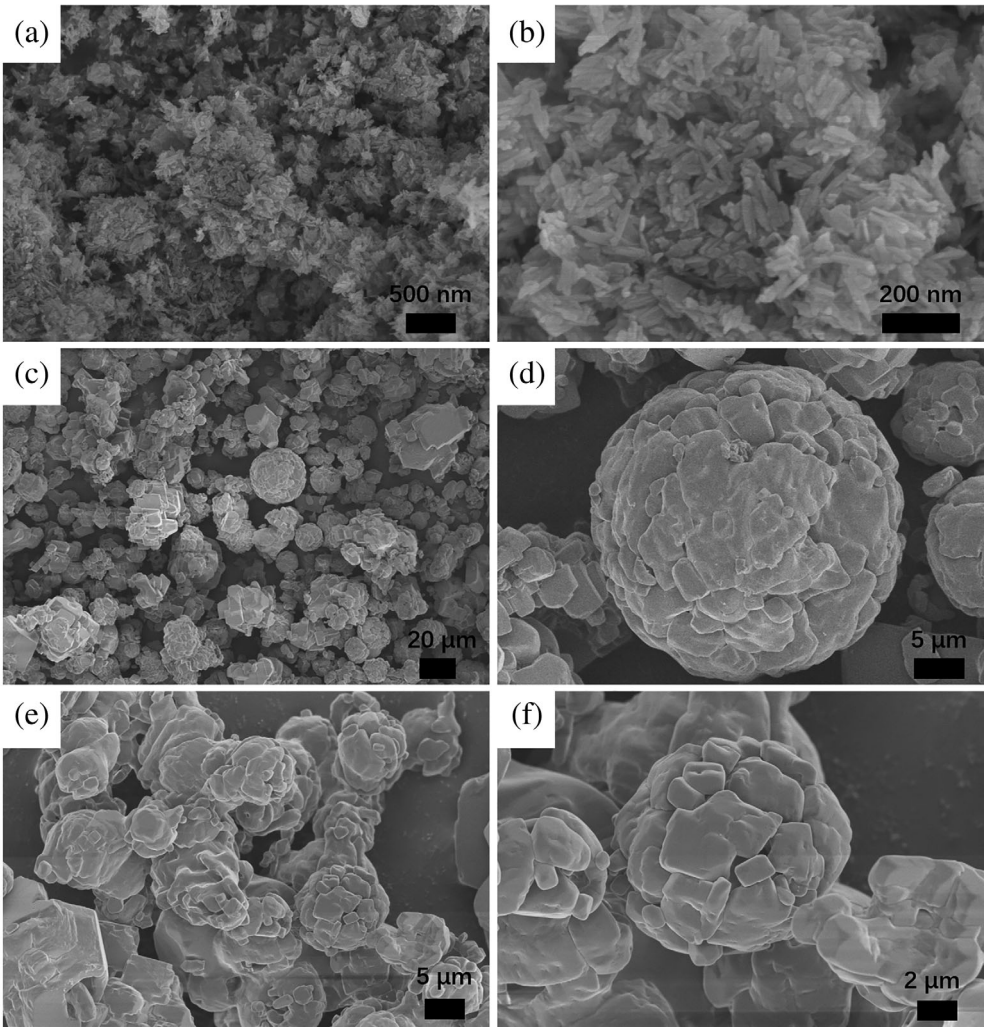

FIGURE 3 SEM images of $_{Ag}$BA microclusters using different magnifications, (a, b): MPs-l; (c, d): MPs-m; (e, f): MPs-h. SEM, scanning electron microscopy

confirming the interactions between BCP nanoparticles and alginate.

Figure 4(b) showed UV–vis absorption bands of $_{Ag}$BA microclusters with using different emulsification power, and the absorption spectra were recorded in the wavelength region of 200–2000 nm. The band from 235 nm to 310 nm exhibited the red-shift at the peak of BCP nanoparticles due to the formation of BCP/Alginate microclusters. The intensity of absorption peaks increased with increasing power. The broad shoulder peak with a maximum at 460 nm was observed, owing to the surface plasmon resonance band (PRB) of the spherical silver nanoparticles incorporated in $_{Ag}$BA microclusters. The UV–vis absorption results were in agreement with FTIR spectra, verifying that the AgNPs were doped in the $_{Ag}$BA microclusters.

The XRD pattern of BCP nanoparticles was exhibited in Figure 4c, and the synthesized BCP nanoparticles were composed of the HA phase and β-TCP phase. The peaks of alginate were observed at $2\theta = 13.7^{\circ}$.[47] In our research, the peak at $2\theta = 13.7^{\circ}$ for MPs-l microclusters was assigned to alginate shown in Figure 4(c). There was a little shift for BCP nanoparticles peaks in the XRD pattern of MPs-l microclusters. Diffraction peaks at $2\theta = 37.4^{\circ}$, 44.5° and 63.4° corresponded well with (1 1 1), (2 0 0), and (2 2 0) plane of the face-centered cubic crystal structure of silver.[48,49] For $_{Ag}$BA microclusters, the XRD pattern overlayed from the peaks of AgNPs, BCP nanoparticles, and alginate, meaning that each component interacted with each other. The above results of FTIR, UV–Vis, and XRD indicated that the strong interaction between the carboxylic group of alginate, calcium ions of BCP nanoparticles, and AgNPs occurred.

3.3 | Antibacterial activity of $_{Ag}$BA microclusters

The Agar-well diffusion method is an effective method to evaluate the antibacterial activity.[50] In our research, the antibacterial activity of $_{Ag}$BA microclusters was carried out against both *E. coli* (Gram-negative) and *S. aureus*

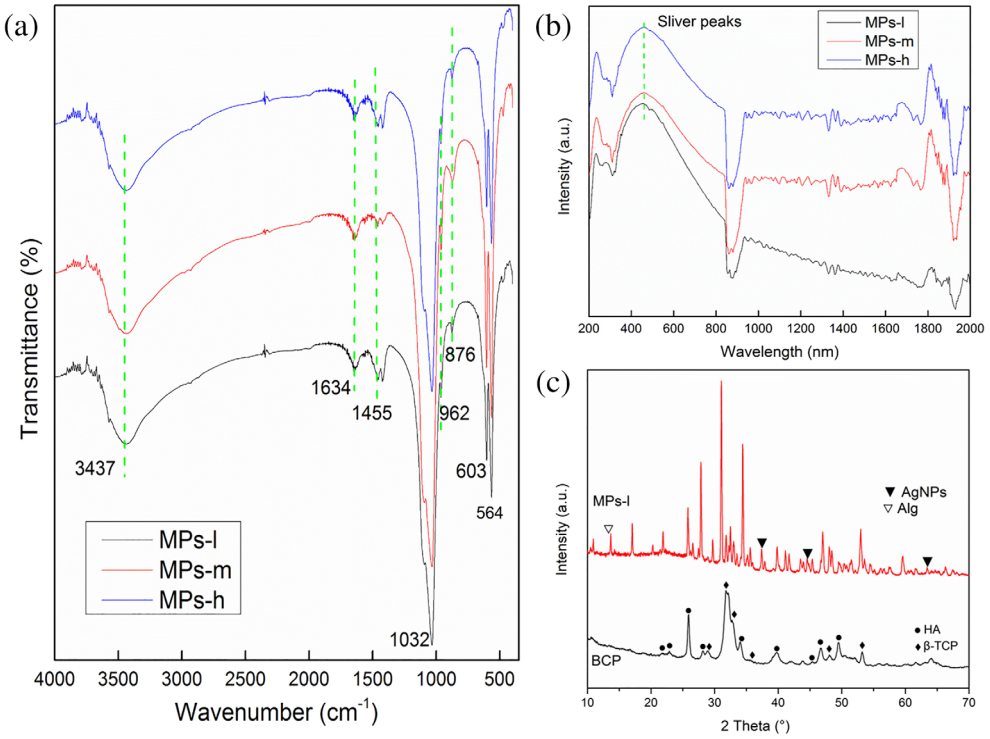

FIGURE 4 (a) FTIR spectra and (b) UV–vis diffuse-reflectance spectra (DRS) of $_{Ag}$BA microclusters; (c) XRD spectra of BCP nanoparticles and MPs-l microclusters. BCP, biphasic calcium phosphate; FTIR, Fourier transform infrared; XRD, X-ray diffraction [Color figure can be viewed at wileyonlinelibrary.com]

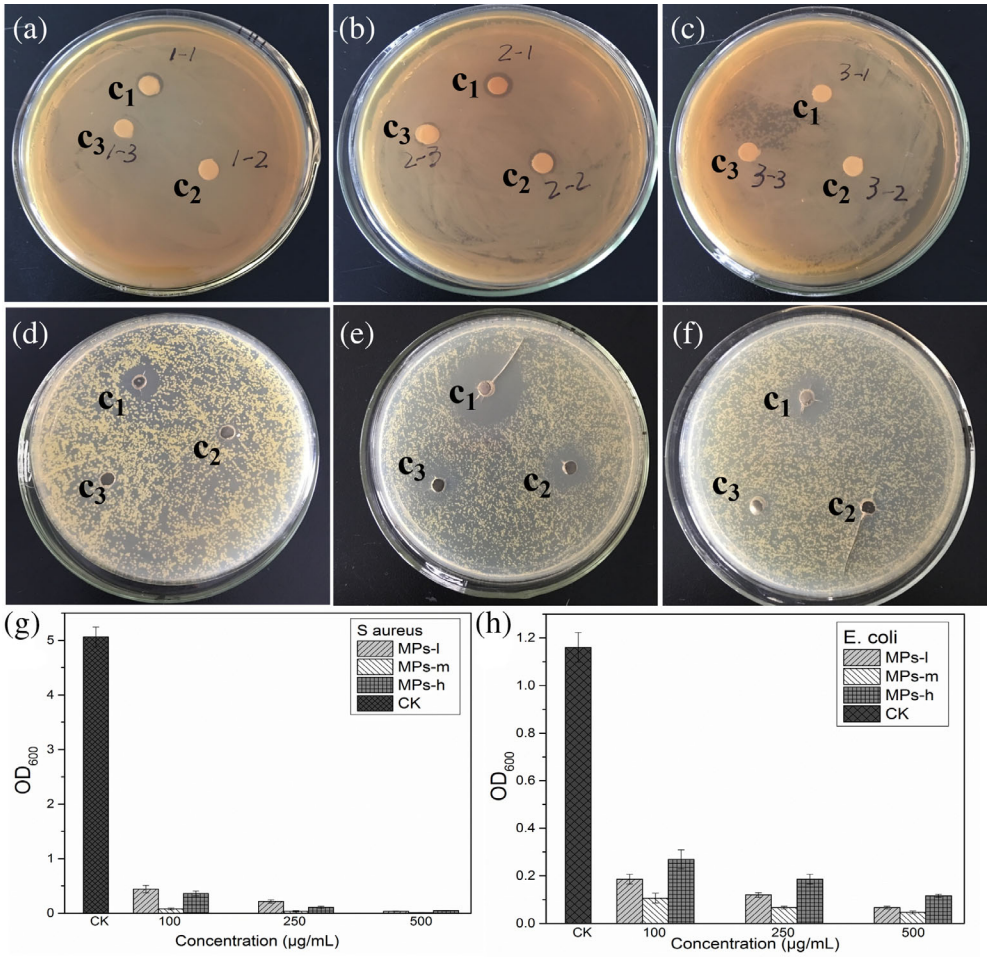

FIGURE 5 The antimicrobial activity of $_{Ag}$BA microclusters, the growth inhibitory effect on gram-negative (*S. aureus*) (a-c) and gram-positive (*E. coli*) (d-f) bacteria grown on nutrient agar plates are evaluated by the size of the inhibitory halo while culturing with $_{Ag}$BA microclusters using different concentration. c_1: 500 μg/ml; c_2: 250 μg/ml; c_3: 100 μg/ml. (a, d): MPs-l; (b, e): MPs-m; (c, f): MPs-h. besides, the optical density at 600 nm (OD_{600nm}) of *S. aureus* (g) and *E. coli* (h) in the Luria-Bertani (LB) medium cultured with $_{Ag}$BA microclusters using different concentrations. *E. coli*, *Escherichia coli*; *S. aureus*, *Staphylococcus aureus* [Color figure can be viewed at wileyonlinelibrary.com]

(Gram-positive) using the above method. As shown in Figure 5, all microclusters exhibited distinct antibacterial activity, which was much more effective than control groups, even at a low concentration (i.e., 100 μg/ml) (Figure 5(g-h)). The larger size and more clear bacteriostatic halos were viewed around $_{Ag}$BA microclusters in Figure 5(a-f), suggesting its excellent inhibition effect with the inhibitory zones over 1 mm. Besides, the microclusters consisting of BCP/alginate were prepared using the same method, and the antimicrobial activity assay confirmed BCP/alginate microclusters did not perform the antibacterial activity against both *E. coli* and *S. aureus*, and the data was not shown here. Overall, $_{Ag}$BA microclusters exhibited good antibacterial activity, especially for MPs-m nanocomposite microclusters.

3.4 | Drug loading and release profile of DOX-loaded $_{Ag}$BA microclusters

The DOX loading efficiency of DOX-loaded $_{Ag}$BA microclusters was shown in Figure 6(a). MPs-m nanocomposite microclusters exhibited a higher loading efficiency of DOX than that of MPs-l and MPs-h. DOX loaded on $_{Ag}$BA microclusters was mainly attributed to the weak electrostatic interaction between $_{Ag}$BA microclusters and DOX molecules. Another critical factor affecting the drug loading efficiency was mainly due to its spherical morphologies related to its surface area. The three-dimensional network structure of microclusters resulted in a much more loaded drug inside.[30] The drug molecules were not only absorbed onto the microclusters' surface but also into the three-dimensional spherical structure of microclusters. MPs-m nanocomposite microclusters could incorporate more DOX molecules into microclusters due to the regular spherical-shape, leading to a higher drug load efficiency.

The release profiles of DOX from DOX-loaded $_{Ag}$BA microclusters in PBS were displayed in Figure 6(b). The MPs-l, MPs-m, and MPs-h microclusters had similar release profiles that exhibited a burst release of 29.6%, 21.8%, and 26.3% within the first 1 h. Then the cumulative release gradually slowed down in the subsequent time with different rates. The initial burst effect was ascribed to the fast release of DOX absorbed on the surface of microclusters. Whereafter, the DOX molecules absorbed inside the microclusters gradually release. Compared with MPs-l and MPs-m, MPs-h nanocomposite microclusters have a better-sustained release effect over an initial period of 8 h. The cumulative release of MPs-h gradually reached a value of 73.3% after 72 h.

3.5 | Cytocompatibility of $_{Ag}$BA microclusters

The CCK-8 assay was employed to evaluate the in vitro cytotoxicity of $_{Ag}$BA microclusters, as shown in Figure 7. The hBMSCs were seeded on microclusters and then cultured for 1, 3, and 5 days. The O.D. values at 450 nm were recorded to quantitively evaluate the growth of the cells cultured with $_{Ag}$BA microclusters. In Figure 7, the hBMSCs cells proliferated with the increase of culturing time, and the cell viability increased while using the microclusters concentration from 100–500 μg/ml, confirming that $_{Ag}$BA microclusters had the pronounced cytocompatibility. The MPs-h microclusters showed a little higher cell proliferation than MPs-l, MPs-m, at different microclusters concentration. Those results confirmed

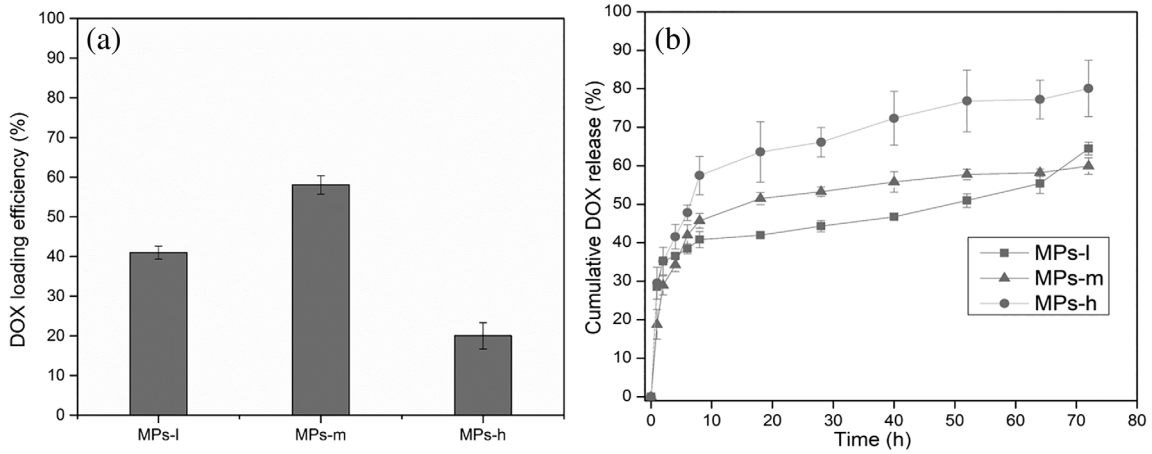

FIGURE 6 (a) DOX loading efficiency of DOX-loaded $_{Ag}$BA microclusters, the release profiles of DOX from DOX-loaded $_{Ag}$BA microclusters in phosphate buffer saline (PBS) at 37 °C for 72 hours. DOX, doxorubicin

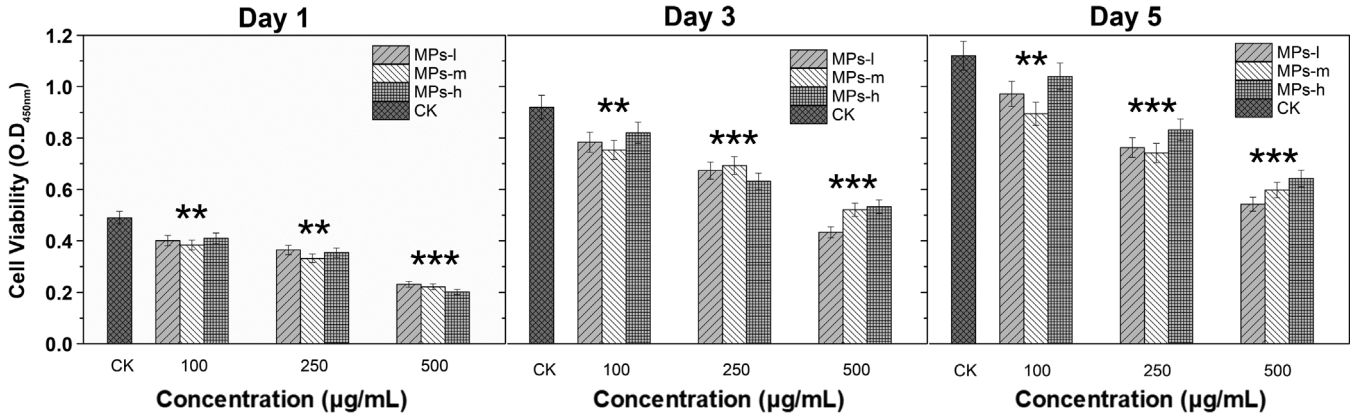

FIGURE 7 Cytocompatibility of $_{Ag}$BA microclusters was evaluated via CCK-8 analysis; the absorbance at 450 nm was recorded after culturing hBMSCs with $_{Ag}$BA microclusters at different days, without adding microclusters as a control group, $^{**}p < 0.01$, $^{***}p < 0.001$. hBMSCs, human bone marrow-derived mesenchymal stem cells

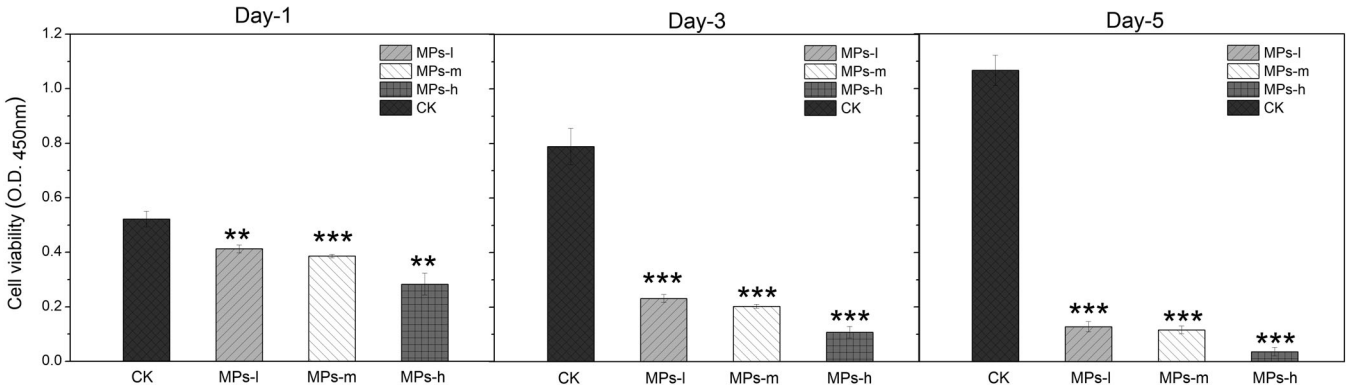

FIGURE 8 Cytotoxicity of DOX loaded $_{Ag}$BA microclusters against A549 cells was evaluated via CCK-8 analysis, the absorbance at 450 nm was tested after culturing A549 cells with DOX loaded $_{Ag}$BA microclusters on different days, without adding microclusters as a control group, $^{**}p < 0.01$, $^{***}p < 0.001$. DOX, doxorubicin

that $_{Ag}$BA microclusters were non-toxic materials that could allow cell attachment and growth.

3.6 | Cytotoxicity of DOX-loaded $_{Ag}$BA microclusters against A549 cells

The cancerous cells were the most widely used to evaluate the cytotoxic potential of DOX loaded materials.[51] The cytotoxic effects of prepared $_{Ag}$BA microclusters were evaluated on the lung cancer cell A549 to demonstrate the inhibition efficiency of DOX-loaded $_{Ag}$BA microclusters on tumor cells (Figure 8). There was a significant decrease in the cell viability of A549 cells after 1, 3, and 5 days of incubation, especially that MPs-h microclusters showed higher cytotoxicity than that of MPs-l and MPs-m. The results indicated that DOX-loaded $_{Ag}$BA microclusters efficiently affected cell viability and induced apoptosis in A549 cells, presenting a better cytotoxic potential against A549 cells.

4 | DISCUSSION

In this work, the silver nanoparticles doped BCP/alginate microclusters were prepared by the double-emulsions method. Compared to mechanical homogenization, the ultrasound-based emulsification technique can produce a much more homogeneous emulsion with smaller droplet size and more stable emulsion while using lower energy consumption and less surfactant. During the preparation of $_{Ag}$BA microclusters, cavitation was formed on the surface of BCP nanoparticles and alginate polymer. Then, the collapse of vapor cavities in the liquid caused the transmitted acoustic energy leading to local high temperature and pressure, and further trigger the strong

interactions between carboxylate group from alginate and phosphate groups in BCP nanoparticles. For the second emulsion of $AgNO_3$ solution and BCP/Alginate microclusters, it has the same phenomenon. Different powers have a significant impact on transmitted acoustic energy, local temperature and pressure, interactions between groups, thus the physicochemical and morphological properties of each microcluster will be influenced. Here, BCP nanoparticles were directly involved in the alginate network to fabricate BCP/Alginate microclusters, then the BCP/alginate microclusters were decorated with AgNPs. During this stage, silver ions penetrated the BCP/alginate matrix. Many hydroxylic and carboxylic groups in the alginate molecules could absorb silver ions through conjugate action,[42] then initiate cross-linking of 1,4′-linked β-D-mannuronic acid and α-L guluronic acid residues in alginate.[52] Subsequently, the AgNPs were in situ incorporated immediately by adding ascorbic acid. During the whole process, ascorbic acid initiated the formation of AgNPs. Meanwhile, calcium ions appeared due to the dissolution of BCP in an acidic environment, which may be cross-link with the alginate molecules and improved the stability of microclusters.[53] Emulsifying power has significant influence on the formation of $_{Ag}$BA microclusters. While using the medium powder (500 W), BCP nanoparticles were entirely impregnated into the alginate network to construct the microclusters with spherical shape (Figure 3(c), (d)). The unsuitable power (300 W, 900 W) affects the dispersion of BCP nanoparticles into alginate network, caused agglomeration behavior, and led to the irregular shape of $_{Ag}$BA microclusters (Figure 3(a-b), (e-f)). The prepared $_{Ag}$BA microclusters could be stored in ultrapure water for couple of weeks. From the DLS results, the hydrated sizes of MPs-l and MPs-h were increased compared with that of MPs-m, proving that MPs-m is much stable than MPs-l and MPs-h. The swelling properties of $_{Ag}$BA microclusters were not performed because it was challenging to obtain such swelling values of $_{Ag}$BA clusters in microsize. However, the zeta potentials of $_{Ag}$BA microclusters were tested, the zeta potential of MPs-m was around −35.8 mV, and the zeta potentials of MPs-l and MPs-h were − 24.3 mV and − 28.2 mV, confirming that MPs-l and MPs-h exhibited more tendency to aggregate and were generally more unstable compared with MPs-m.

It has been well-established that BCP, as synthetic CaP bioceramics, has good biocompatibility and non-immune response.[54] Due to the lower toxicity for human cells, inhibiting aerobic respiration, damaging DNA,[55,56] AgNPs, synthesized by chemical reduction, photoreduction, and green one-step,[57–59] have been widely applied in the treatment of bacterial infection. All of these endows the $_{Ag}$BA microclusters with good antibacterial properties (Figure 5) and cytocompatibility (Figure 7). Drug-loaded microclusters provide complementary benefits in dealing with the disease.[60] DOX is considered one of the most effective agents as an anthracycline antibiotic[61] which is the main antibacterial constituent and plays an essential role in the microclusters. DOX released from DOX-loaded $_{Ag}$BA microclusters could be explained as ion exchange. Here, The abundant salt solutions with minimum concentration have a greater effect on the fraction released. Moreover, the concentration of Na^+ ions was expected to have a significant impact on in vitro DOX release. The microclusters contain negatively charged alginate and DOX is a cationic amphiphile molecule. The counterions in the release medium has the ability to control the drug release.

Furthermore, the cell viability of $_{Ag}$BA microclusters decreased after loading the DOX (Figure 8) because DOX impairs DNA synthesis and cell membranes by intercalating between DNA bases and generating free radicals.[62,63] The DOX molecules were not only absorbed into the inside of microclusters but also on the surface of microclusters. During the DOX release, three-stage can take place: (1) the fast release of DOX molecules absorbed on the microclusters' surface corresponding to the burst effect; (2) the sustained release behavior of the drug absorbed inside the microclusters; (3) the slight release from the degradation of DOX. Besides, the deprotonation of carboxyl groups of alginate also results in microclusters restructure and higher DOX release at the beginning.[64] The DOX loading efficiency, the release profiles of DOX-loaded $_{Ag}$BA microclusters, and cell viability indicate that drug molecules could be effectively loaded and released. Thus, our findings pointed out that $_{Ag}$BA microclusters have the potential applications for designing the antibacterial drug-loading system for treating bone-related diseases.

5 | CONCLUSIONS

In summary, $_{Ag}$BA microclusters were successfully synthesized using the double-emulsions method. The AgNPs were distributed in the entire $_{Ag}$BA microclusters evenly. The antibacterial test and cytocompatibility indicated that $_{Ag}$BA microclusters were effective in inhibiting the growth of Gram-positive *S. aureus and* Gram-negative *E. coli*. The DOX-loaded AgNPs-doped BCP/Alginate microclusters presented a burst release rate at first 1 h, then the cumulative release gradually slower down in the subsequent time with different rates. The cumulative release of MPs-h gradually reached a value of 73.3% after 72 h. Therefore, the nanocomposite $_{Ag}$BA microclusters

are excellent antibacterial materials and drug carriers with great application potentials for development as a new strategy for cancer therapy, especially in the treatment of bone-related diseases.

ACKNOWLEDGMENTS

This research was supported by the National Natural Science Foundation of China (31700840). The authors would like to acknowledge the Nanhu Scholars Program for Young Scholars of XYNU, "333 High-level Talent Training Project" of the Jiangsu Province (2019, 05). Lei Nie and Yaling Deng contributed equally to this work and considered as co-first authors.

CONFLICT OF INTEREST

The authors declare that they have no known competing financial interests or personal relationships that could have appeared to influence the work reported in this paper.

ORCID

Lei Nie https://orcid.org/0000-0002-6175-5883

REFERENCES

[1] A. Raghuram, A. Singh, D. K. Chang, M. Nunez, E. M. Reece, *Semin. last. Surg.* **2019**, *33*, 190.
[2] L. Nie, P. Zou, S. B. Feng, J. P. Suo, *J. Mater. Sci.: Mater. Med.* **2013**, *24*, 689.
[3] D. Chen, C. X. Zhang, H. J. Huo, C. C. Ji, M. Sun, L. Nie, *Mater. Lett.* **2018**, *229*, 138.
[4] M. H. Hong, S. M. Kim, Y. K. Lee, J. Ceram, *Sci. Technol.* **2017**, *8*, 541.
[5] A. Shavandi, A. E. D. A. Bekhit, M. A. Ali, Z. F. Sun, *Int. J. Biol. Macromol.* **2015**, *80*, 445.
[6] W. T. Dang, B. Ma, Z. G. Huan, R. C. Lin, X. Y. Wang, T. Li, J. F. Wu, N. Ma, H. B. Zhu, J. Chang, C. T. Wu, *Appl. Mater. Today.* **2019**, *16*, 42.
[7] E. M. Hetrick, M. H. Schoenfisch, *Chem. Soc. Rev.* **2006**, *35*, 780.
[8] G. D. Venkatasubbu, S. Ramasamy, V. Ramakrishnan, J. Kumar, *3 BioTechniques* **2011**, *1*, 173.
[9] L. Benedini, J. Laiuppa, G. Santillán, M. Baldini, P. Messina, *Mater. Sci. Eng., C* **2020**, *115*, 111101.
[10] E. Vorndran, M. Geffers, A. Ewald, M. Lemm, B. Nies, U. Gbureck, *Acta Biomater.* **2013**, *9*, 9558.
[11] M. M. Alam, M. Islam, A. Wahab, M. Billah, *J Med.* **2019**, *20*, 38.
[12] J. M. A. Blair, M. A. Webber, A. J. Baylay, D. O. Ogbolu, L. J. V. Piddock, *Nat. Rev. Microbiol.* **2015**, *13*, 42.
[13] J. J. Castellano, S. M. Shafii, F. Ko, G. Donate, T. E. Wright, R. J. Mannari, W. G. Payne, D. J. Smith, M. C. Robson, *Int. Wound. J.* **2007**, *4*, 114.
[14] J. Yan, A. M. Abdelgawad, M. E. El-Naggar, O. J. Rojas, *Carbohydr. Polym.* **2016**, *147*, 500.
[15] M. Uno, M. Kurachi, N. Wakamatsu, Y. Doi, *J. Prosthet. Denti.* **2013**, *109*, 241.
[16] J. R. Morones-Ramirez, J. A. Winkler, C. S. Spina, J. J. Collins, *Sci. Transl. Med.* **2013**, *5*, 190ra81.
[17] Y. J. Cheng, D. N. Zeiger, J. A. Howarter, X. R. Zhang, N. J. Lin, J. M. Antonucci, S. Lin-Gibson, *J. Biomed. Mater. Res. B Appl. Biomater.* **2011**, *97*, 124.
[18] S. S. D. Kumar, N. K. Rajendran, N. N. Houreld, H. Abrahamse, *Int. J. Biol. Macromol.* **2018**, *115*, 165.
[19] S. Kar, B. Bagchi, S. Bhandary, R. Basu, P. Nandy, S. Das, *Biochim. Biophys. Acta* **2014**, *1840*, 3264.
[20] B. J. Chen, Y. F. Jiang, M. L. Zhao, W. N. Wang, Z. Y. Chu, R. H. Huo, F. Hu, W. Zhou, T. He, H. S. Qian, *Mater. Lett.* **2020**, *262*, 127057.
[21] B. Z. Zheng, L. Qian, H. Y. Yuan, D. Xiao, X. P. Yang, M. C. Paau, M. M. F. Choi, *Talanta* **2010**, *82*, 177.
[22] X. Y. Li, Z. X. Cai, D. U. Ahn, X. Huang, *Colloids Surf., B* **2019**, *183*, 110449.
[23] Q. J. Zhou, T. W. Wang, C. Wang, Z. Wang, Y. N. Yang, P. Li, R. H. Cai, M. Sun, H. Y. Yuan, L. Nie, *Colloids Surf., A* **2020**, *585*, 124081.
[24] Y. Shao, C. Wu, T. Wu, C. Yuan, S. Chen, T. Ding, X. Ye, Y. Hu, *Int. J. Biol. Macromol.* **2018**, *111*, 1281.
[25] R. E. Webber, K. R. Shull, *Macromolecules* **2004**, *37*, 6153.
[26] S. A. Piletsky, A. P. F. Turner, *Electroanalysis* **2002**, *14*, 317.
[27] A. Turlybekuly, A. D. Pogrebnjak, L. F. Sukhodub, L. B. Sukhodub, A. S. Kistaubayeva, I. S. Savitskaya, D. H. Shokatayeva, O. V. Bondar, Z. K. Shaimardanov, S. V. Plotnikov, B. H. Shaimardanova, I. Digel, *Mater. Sci. Eng., C* **2019**, *104*, 109965.
[28] S. Potiwiput, H. P. Tan, G. L. Yuan, S. K. Li, T. L. Zhou, J. L. Li, Y. Jia, D. S. Xiong, X. H. Hu, Z. H. Ling, Y. Chen, *Mater. Chem. Phys.* **2020**, *241*, 122354.
[29] J. Jin, M. Xu, Y. X. Liu, Z. X. Ji, K. L. Dai, L. Zhang, L. Wang, F. Ye, G. Chen, Z. B. Lv, *Colloids Surf., B* **2020**, *194*, 111168.
[30] Y. G. Bi, Z. T. Lin, S. T. Deng, *Mater. Sci. Eng., C* **2019**, *100*, 576.
[31] H. B. Li, F. Jiang, S. Ye, Y. Y. Wu, K. P. Zhu, D. P. Wang, *Mater. Sci. Eng., C* **2016**, *62*, 779.
[32] L. Nie, C. Wang, R. X. Hou, X. Y. Li, M. Sun, J. P. Suo, Z. Wang, R. H. Cai, B. W. Yin, L. Fang, X. Y. Wei, H. Y. Yuan, *SN Appl. Sci.* **2019**, *1*, 545.
[33] Z. R. Tong, J. Y. Yang, L. Z. Lin, R. Q. Wang, B. Cheng, Y. Chen, L. S. Tang, J. Y. Chen, X. L. Ma, *Carbohydr. Polym.* **2019**, *221*, 21.
[34] G. Daculsi, *Biomaterials* **1998**, *19*, 1473.
[35] L. Nie, Q. Y. Wu, H. Y. Long, K. H. Hu, J. Biomater, *Sci., Polym. Ed* **2019**, *30*, 1636.
[36] L. Nie, Y. L. Deng, P. Li, R. X. Hou, A. Shavandi, S. F. Yang, *ACS Omega* **2020**, *5*, 10948.
[37] R. Fernandes, P. Siegel, S. Komarova, J. Hiltion, C. Addison, M. F. K. Ibrahim, J. Werier, K. Dennis, G. Singh, E. Amir, V. Jarvis, U. Emmenegger, S. Mazzarello, M. Clemons, J. Bone, *Oncol.* **2016**, *5*, 57.
[38] I. Zarkesh, M. H. Ghanian, M. Azami, F. Bagheri, H. Baharvand, J. Mohammadi, M. B. Eslaminejad, *Colloids Surf., B* **2017**, *157*, 223.
[39] H. V. Ho, G. Tripathi, J. Gwon, S. Y. Lee, B. T. Lee, *Mater. Des.* **2020**, *194*, 108892.
[40] C. F. Marques, S. M. Olhero, P. M. C. Torres, J. C. C. Abrantes, S. Fateixa, H. I. S. Nogueira, I. A. C. Ribeiro, A. Bettencourt,

A. Sousa, P. L. Granja, J. M. F. Ferreira, *Mater. Sci. Eng., C* **2019**, *94*, 426.
[41] E. Lengert, A. M. Yashchenok, V. Atkin, A. Lapanje, D. A. Gorin, G. B. Sukhorukov, B. V. Parakhonskiy, *RSC Adv.* **2016**, *6*, 20447.
[42] L. Nie, D. Chen, J. Fu, S. H. Yang, R. X. Hou, J. P. Suo, *Biochem. Eng. J.* **2015**, *98*, 29.
[43] L. Nie, D. Chen, J. P. Suo, P. Zou, S. B. Feng, Q. Yang, S. H. Yang, S. N. Ye, *Colloids Surf., B* **2012**, *100*, 169.
[44] S. Kondaveeti, P. V. A. Bueno, A. M. Carmona-Ribeiro, F. Esposito, N. Lincopan, M. R. Sierakowski, D. F. S. Petri, *Carbohydr. Polym.* **2018**, *186*, 159.
[45] C. Sartori, D. S. Finch, B. Ralph, K. Gilding, *Polymer* **1997**, *38*, 43.
[46] J. Wang, Y. Y. Su, L. Z. Xu, D. Y. Li, *Mater. Sci. Eng., C* **2020**, *116*, 111220.
[47] J. W. Li, J. W. Ma, S. J. Chen, J. M. He, Y. D. Huang, *Food Hydrocolloids* **2018**, *82*, 363.
[48] M. S. A. S. Shah, K. Zhang, A. R. Park, K. S. Kim, N. G. Park, J. H. Park, P. J. Yoo, *Nanoscales* **2013**, *5*, 5093.
[49] P. Bazant, I. Kuritka, L. Munster, L. Kalina, *Cellulose* **2015**, *22*, 1275.
[50] M. Balouiri, M. Sadiki, S. K. Ibnsouda, J. Pharm, *Anal.* **2016**, *6*, 71.
[51] M. Y. Alfaifi, A. A. Shati, S. E. I. Elbehairi, U. A. Fahmy, N. A. Alhakamy, S. Md, *3 Biotech* **2020**, *10*, 133.
[52] K. S. Khairou, R. M. Hassan, *High Perform. Polym.* **2002**, *14*, 93.
[53] E. Lengert, B. Parakhonskiy, D. Khalenkow, A. Zečić, M. Vangheel, J. M. M. Moreno, B. P. Braeckman, A. G. Skirtach, *Nanoscale* **2018**, *10*, 17249.
[54] N. Broggini, D. D. Bosshardt, S. S. Jensen, M. M. Bornstein, C. C. Wang, D. Buser, *J. Biomed. Mater. Res. B. Appl. Biomater.* **2015**, *103*, 1478.
[55] T. Y. Shi, X. S. Sun, Q. Y. He, *Curr. Protein Pept. Sci.* **2018**, *19*, 525.
[56] C. Greulich, D. Braun, A. Peersch, J. Diendorf, B. S. M. Epple, M. Köller, *RSC Adv.* **2012**, *2*, 6981.
[57] M. Mohammadlou, H. Maghsoudi, H. Jafarizadeh-Malmiri, *Int Food Res J.* **2016**, *23*, 446.
[58] S. H. Lee, B. H. Jun, *Int. J. Mol. Sci.* **2019**, *20*, 865.
[59] T. W. Wang, F. Zhang, R. Zhao, C. Wang, K. H. Hu, Y. Sun, C. Politis, A. Shavandi, L. Nie, *Des. Monomers Polym.* **2020**, *23*, 118.
[60] S. B. Feng, L. Nie, P. Zou, J. P. Suo, *J. Microencapsulation* **2015**, *32*, 201.
[61] F. Arcamone, G. Cassinelli, G. Fantini, A. Grein, P. Orezzi, C. Pol, C. Spalla, *Biotechnol. Bioeng.* **2000**, *67*, 704.
[62] S. W. Wang, S. Kotamraju, E. Konorev, S. Kalivendi, J. Joseph, B. Kalyanaraman, *Biochem. J.* **2002**, *367*, 729.
[63] R. L. Momparler, M. Karon, S. E. Siegel, F. Avila, *Cancer Res.* **1976**, *36*, 2891.
[64] L. Lacerda, A. L. Parize, V. Fávere, M. C. M. Laranjeira, H. K. Stulzer, *Mater. Sci. Eng. C.* **2014**, *39*, 161.

How to cite this article: Nie L, Deng Y, Zhang Y, et al. Silver-doped biphasic calcium phosphate/alginate microclusters with antibacterial property and controlled doxorubicin delivery. *J Appl Polym Sci*. 2020;e50433. https://doi.org/10.1002/app.50433